

Solidification of an alloy cooled from above Part 2. Non-equilibrium interfacial kinetics

By ROSS C. KERR¹†, ANDREW W. WOODS^{1,2},
M. GRAE WORSTER¹‡ AND HERBERT E. HUPPERT^{1,2}

¹Department of Applied Mathematics and Theoretical Physics,

²Institute of Theoretical Geophysics,

University of Cambridge, Silver Street, Cambridge CB3 9EW, UK

(Received 22 June 1989)

The model developed in Part 1 for the solidification and convection that occurs when an alloy is cooled from above is extended to investigate the role of disequilibrium at the mush–liquid interface. Small departures from equilibrium are important because in a convecting system an interfacial temperature below its equilibrium value can drive the bulk temperature of the melt below its liquidus. This behaviour is observed in experiments and can result in crystallization within and at the base of the convecting melt. The additional crystals formed in the interior can settle to the base of the fluid and continue to grow, causing the composition of the melt to change. This ultimately affects the solidification at the roof. The effects of disequilibrium are explored in this paper by replacing the condition of marginal equilibrium at the interface used in the model of Part 1 with a kinetic growth law of the form $\dot{h}_1 = \mathcal{G}\delta T$, where \dot{h}_1 is the rate of advance of the mush–liquid interface, δT is the amount by which the interfacial temperature is below the liquidus temperature of the melt and \mathcal{G} is an empirical constant. This modification enables the model to predict very accurately both the growth of the mushy layer and the development of supersaturation in the isopropanol experiments described in Part 1. An additional series of experiments, using aqueous solutions of sodium sulphate, is presented in which the development of supersaturation leads to the internal nucleation and growth of crystals. A further extension of the model is introduced which successfully accounts for this internal crystal growth and the changing composition of the melt. We discuss the implications of this work for geologists studying the formation of igneous rocks. Important conclusions include the facts that cooling the roof of a magma chamber can lead to crystallization at its floor and that vigorous convection can occur in a magma chamber even when there is no initial superheat.

1. Introduction

When a melt is cooled at a surface forming part of its boundary, it can crystallize at positions that are remote from the cooled surface. We and others (e.g. Chen & Turner 1980; Turner, Huppert & Sparks 1986) have observed such behaviour in laboratory experiments in which aqueous solutions of various salts were cooled from

† Present address: Research School of Earth Sciences, ANU, GPO Box 4, Canberra, ACT 2601, Australia.

‡ Present address: Departments of Engineering Sciences and Applied Mathematics, and Chemical Engineering, Northwestern University, Evanston, IL 60208, USA.

horizontal surfaces forming the upper boundaries of their containers. In addition to the expected solidification of crystals attached to the cooling plate, crystallization took place at the floor of the container, probably seeded by small crystals that had fallen from the roof. In order for this additional solidification to take place, the melts must have become supersaturated during the course of the experiments. Such behaviour has important consequences for the solidification of alloys and is inexplicable by any theory constrained by the assumption of equilibrium thermodynamics.

As a liquid solidifies, the temperature at the interface between the liquid and the growing solid must necessarily be less than the equilibrium, freezing temperature of the liquid. Often, the departure from equilibrium is small and the solidification process can be accurately modelled by assuming that all the phase boundaries are at precisely their equilibrium temperatures. This is the approach taken in classical studies of the solidification of pure melts (see Carslaw & Jaeger 1959, for example), and is used to good effect in recent theories of the solidification of alloys (Huppert & Worster 1985; Worster 1986; Woods & Huppert 1989). In Part 1 of this series of papers (Kerr *et al.* 1990*a*), we used equilibrium theory to analyse many of the phenomena that can occur when a two-component melt is cooled from above, and we applied our results to the particular case of ice freezing from aqueous solutions of isopropanol. Since the ice crystals that formed were less dense than the solution, no seed crystals fell from the roof and the only solidification that took place was the directional growth of a mushy layer adjacent to the upper, cooled boundary. The theoretical model developed in Part 1, which was based on equilibrium thermodynamics, was able to predict the growth of the mushy layer to a high degree of accuracy. It was noticed, however, that the liquid region below the mushy layer in the experiments became supersaturated, though no new ice crystals were observed to nucleate either in the interior or on the floor.

Guided by the experiments reported in Part 1 and by the results of more detailed experiments described in §2 of this paper, in which we focus on conditions at the interface between mush and liquid, we modify our theoretical model to take account of disequilibrium at the interface. The condition of marginal equilibrium is replaced by a simple kinetic growth law that relates the rate of growth of a crystal to the local supersaturation in the melt. We show that this modification has little effect on the classical theories of solidification, in which heat transfer is solely by conduction. Its effect is merely to change the temperature of the interface by an amount which is negligible in most circumstances.

The modification makes a fundamental difference, however, when the melt is convecting, since supersaturated fluid can be advected from the interface into the whole body of the melt. Thereby the whole of the liquid region can become supersaturated. This is in accordance with the experimental observations reported in Part 1. In §3, we incorporate the new interfacial condition into the theoretical model for the whole convecting system and obtain significantly better agreement with the experimental results of Part 1 than was achieved there.

In §4 we describe a new set of quantitative experiments in which aqueous solutions of sodium sulphate were cooled from above. Crystals of sodium sulphate decahydrate ($\text{Na}_2\text{SO}_4 \cdot 10\text{H}_2\text{O}$) formed to release buoyant residual fluid as before. However, in this case, the crystals are denser than the solution and some did grow from the floor into the supersaturated, convecting liquid region in addition to those formed at the roof. An extension of our theoretical model, which takes account of this additional crystal growth, is formulated and solved. Good agreement between the results of the

extended model and the experimental observations is shown to be possible by a suitable choice of the kinetic growth parameter.

Some discussion of the importance of our results in the fields of metallurgy and geology is made in §5, though a more comprehensive development of the results applied to systems that solidify completely is presented in Part 3 of this series (Kerr *et al.* 1990*b*).

2. An interfacial growth law

In Part 1, a model of the growth of a mushy layer was developed in which the temperature at the mush-liquid interface was equal to the liquidus temperature of the underlying, convecting liquid. However, this condition, which derives from a condition of marginal equilibrium, can only be approximately correct since crystal growth is necessarily a non-equilibrium process. Crystals can only grow in a liquid that is locally supersaturated, and will grow at a rate that depends upon the magnitude of the supersaturation.

Measurements have been made for many crystals of the relationship between their growth rate and the local supersaturation (Kurz & Fisher 1986), and many different results have been obtained. A simple case to envisage is a linear growth law of the form

$$\dot{h}_i = \mathcal{G}(T_L - T_i), \quad (2.1)$$

where $T_L = T_L(C_f)$ is the liquidus temperature of the liquid region, T_i is the temperature of the interface, and the 'kinetic growth parameter' \mathcal{G} is a constant associated with activation energy required for atomic attachment to the growing crystal face. We repeated the isopropanol experiment of Part 1 several times, and carefully measured $h_i(t)$ and T_i as the interface passed a number of fixed thermistors inserted into the tank. We fitted the data of h_i versus time using a regression technique involving cubic splines, and determined \dot{h}_i from the best-fit curve. Values of \dot{h}_i versus $T_L - T_i$, obtained in this way, are shown in figure 1. We see that the data are reasonably consistent with the linear form (2.1), and we estimate \mathcal{G} from the solid line to be $2.2 \times 10^{-4} \text{ cm } ^\circ\text{C}^{-1} \text{ s}^{-1}$. The dashed lines correspond to an overestimate (\mathcal{G}_+) and an underestimate (\mathcal{G}_-) of \mathcal{G} by 40%. They will be used later to show that the value of \mathcal{G} does not have to be known very accurately in order to predict the evolution of our experiments. The measurements are all in the range $0 < T_L - T_i < 3^\circ\text{C}$ but we shall later assume that the same linear relationship holds for larger supersaturations. We shall see, however, that levels of supersaturation in excess of 3°C exist only at very early times (less than about 10 min) in the experiments.

Before incorporating (2.1) into the full analytical model of Part 1, we consider the general properties of (2.1) and its effect on equilibrium models of solidification. If we make (2.1) dimensionless with respect to scales appropriate to thermal diffusion, the dimensionless growth parameter

$$\gamma = \frac{\Delta TH}{\kappa_\ell} \mathcal{G} \quad (2.2)$$

emerges, where κ_ℓ is the thermal diffusivity of the melt, ΔT is the difference between the temperature of the cooled boundary T_b and the initial liquidus temperature of the melt T_L , and H is a typical dimension of the system. In our experiments, γ has a value of about 80. If γ is treated as a large parameter then (2.1) indicates that the growth rates are rapid compared with thermal diffusion rates if the supersaturation is $O(\Delta T)$. Conversely, if, as in the current situation, heat transfer is the rate controlling process then the large value of γ indicates that the degree of supersaturation is small. This

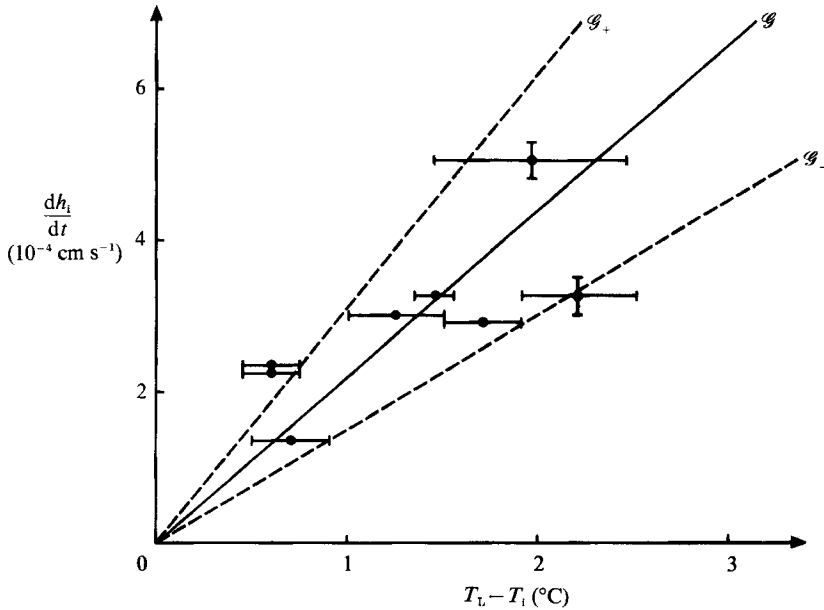


FIGURE 1. Experimental measurements of interfacial undercooling ($T_L - T_i$) versus interfacial growth velocity \dot{h}_i for a 16.8 wt% aqueous solution of isopropanol. The solid line denotes the interfacial growth law corresponding to an estimate of the kinetic growth parameter \mathcal{G} of $2.2 \times 10^{-4} \text{ cm } ^\circ\text{C}^{-1} \text{ s}^{-1}$. The dashed lines denote interfacial growth laws corresponding to an overestimate (\mathcal{G}_+) and an underestimate (\mathcal{G}_-) of \mathcal{G} by 40%.

gives support to the usual approximation of equilibrium thermodynamics. Indeed it is perhaps more instructive to think of (2.1) not as a growth law but as an equation for the kinetic undercooling

$$T_L - T_i = \mathcal{G}^{-1} \dot{h}_i, \quad (2.3)$$

which is small compared with ΔT when γ is small. Asymptotically, in the limit $\gamma \gg 1$, the incorporation of (2.1) into diffusion-controlled equilibrium models will only change the results significantly at very early times ($t = O(\gamma^{-2} H^2 / \kappa_l)$), where the singular growth rate, of $O((\kappa_l / t)^{1/2})$, becomes bounded above by $\mathcal{G}(T_L - T_b)$.

3. The full theoretical model

A model for the growth of a mushy layer formed by cooling an alloy from above is illustrated in figure 2. A mushy layer extends from the roof, at $z = 0$, to $z = h_i(t)$ where the temperature is equal to T_i . In Part 1, the condition of marginal equilibrium (Worster 1986), applied at the interface between the mushy layer and the convecting liquid below it, required that T_i was equal to $T_L(C_0)$, the liquidus temperature in the liquid region. Here, in contrast, $T_i < T_L$ in order that \dot{h}_i is positive according to (2.1). One consequence of this disequilibrium at the interface is that the solid fraction is no longer zero at the edge of the mushy layer. This feature was noted by Flood & Hunt (1987), who used a kinetic growth law in a model of the columnar-equiaxed transition in metallic alloys. As in Part 1, we assume that the interior of the mushy layer is in local thermodynamic equilibrium and that the same equations govern its evolution. Therefore, the dimensionless temperature

$$\theta = \frac{T - T_L(C_0)}{\Delta T}, \quad (3.1)$$

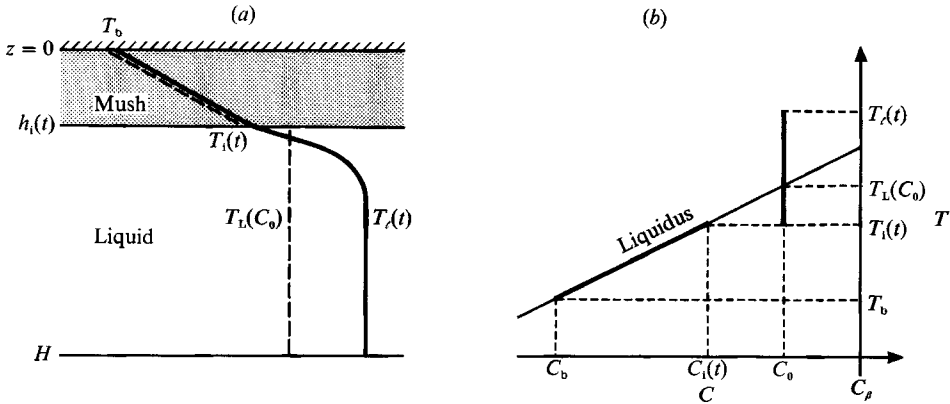


FIGURE 2. Definition sketches for the model outlined in §3: a model (a), and corresponding equilibrium phase diagram (b), for the growth of a mushy layer below a cold, horizontal boundary maintained at a fixed temperature T_b . Throughout the mushy layer, the temperature (solid line) is constrained to equal the liquidus temperature (dashed line) of the interstitial melt. The interfacial temperature T_i is less than the equilibrium freezing temperature of the melt $T_L(C_0)$. Vigorous convection in the melt keeps its temperature uniform.

where $\Delta T = T_L(C_0) - T_b$, satisfies the nonlinear diffusion equation

$$c \frac{\partial \theta}{\partial t} = \frac{\partial}{\partial z} \left(k \frac{\partial \theta}{\partial z} \right) \quad (0 \geq z \geq h_1), \quad (3.2)$$

in which lengths have been scaled with the height of the container H , time has been scaled with H^2/κ_ℓ and the variable coefficients are given by

$$k = \phi \frac{k_\beta}{k_\ell} + (1 - \phi) \quad (3.3)$$

and

$$c = \phi \frac{c_\beta}{c_\ell} + (1 - \phi) + \frac{S}{\mathcal{L}} (1 - \phi)^2, \quad (3.4)$$

where

$$\phi = \frac{-\theta}{\mathcal{L} - \theta}, \quad (3.5)$$

$$S = \frac{\mathcal{L}}{c_\ell \Delta T}, \quad (3.6)$$

and

$$\mathcal{L} = \frac{C_\beta - C_0}{C_0 - C_b} \quad (3.7)$$

(see Part 1). Equation (3.2) is subject to the boundary conditions

$$\theta = -1 \quad (z = 0) \quad (3.8)$$

and

$$\theta = \theta_1 \quad (z = h_1(t)). \quad (3.9)$$

The unknown temperature θ_1 is incorporated within the interfacial growth law introduced in §2, which can be written in the dimensionless form

$$\dot{h}_1 = -\gamma \theta_1. \quad (3.10)$$

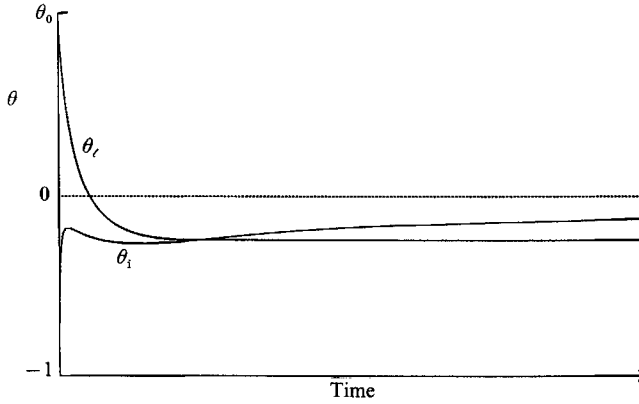


FIGURE 3. The schematic behaviour of the dimensionless temperatures at the interface θ_i , and in the liquid θ_l , for the model given in §3.

The equations expressing conservation of heat at the interface

$$\{S\phi_i + (\theta_l - \theta_i)\} \dot{h}_i = k \frac{\partial \theta}{\partial z} \Big|_{h_i^-} - Nu(\theta_l - \theta_i)^{\frac{4}{3}}, \quad (3.11)$$

and the evolution of the melt temperature

$$(1 - h_i) \dot{\theta}_l = -Nu(\theta_l - \theta_i)^{\frac{4}{3}} \quad (3.12)$$

are similar to those derived in Part 1 (equations (3.19) and (3.20)), though they now involve the variable θ_i and, as mentioned earlier, ϕ_i is no longer equal to zero. The Nusselt number appearing in (3.11) and (3.12) is defined by

$$Nu = 2^{\frac{3}{2}} \lambda (\alpha g \Delta T H^3 / \kappa_l \nu)^{\frac{1}{2}}, \quad (3.13)$$

where α is the thermal expansion coefficient, ν the kinematic viscosity, g the acceleration due to gravity and λ is a constant.

We solved (3.2) numerically using the implicit method outlined in Part 1, subject to the boundary conditions (3.8) and (3.9) while θ_i was varied in a combined secant/binary search, root-finding algorithm until the equation

$$-\{S\phi_i + (\theta_l - \theta_i)\} \gamma \theta_i = k \frac{\partial \theta}{\partial z} \Big|_{h_i^-} - Nu(\theta_l - \theta_i)^{\frac{4}{3}}, \quad (3.14)$$

obtained by combining (3.10) and (3.11), was satisfied to sufficient accuracy. The position of the interface and the temperature of the environment were then updated according to (3.10) and (3.12), starting from initial values $h_i = 0$ and $\theta_l = \theta_0 \equiv (T_0 - T_L(C_0)) / \Delta T$. As we shall see from the results, it is possible for the temperature of the interface θ_i to become greater than the temperature of the liquid θ_l once the latter has dropped below the liquidus value $\theta = 0$. When this occurred, the convective heat flux $Nu(\theta_l - \theta_i)^{\frac{4}{3}}$ was set to zero on the grounds that the temperature field is then gravitationally stable. Note that the conductive flux from the melt to the mushy layer is always included in the analysis. It is represented by the term $\theta_l - \theta_i$ within the curly brackets in (3.14). The conductive flux from the melt serves only to cool the advancing thermal boundary layer and cannot affect the bulk temperature

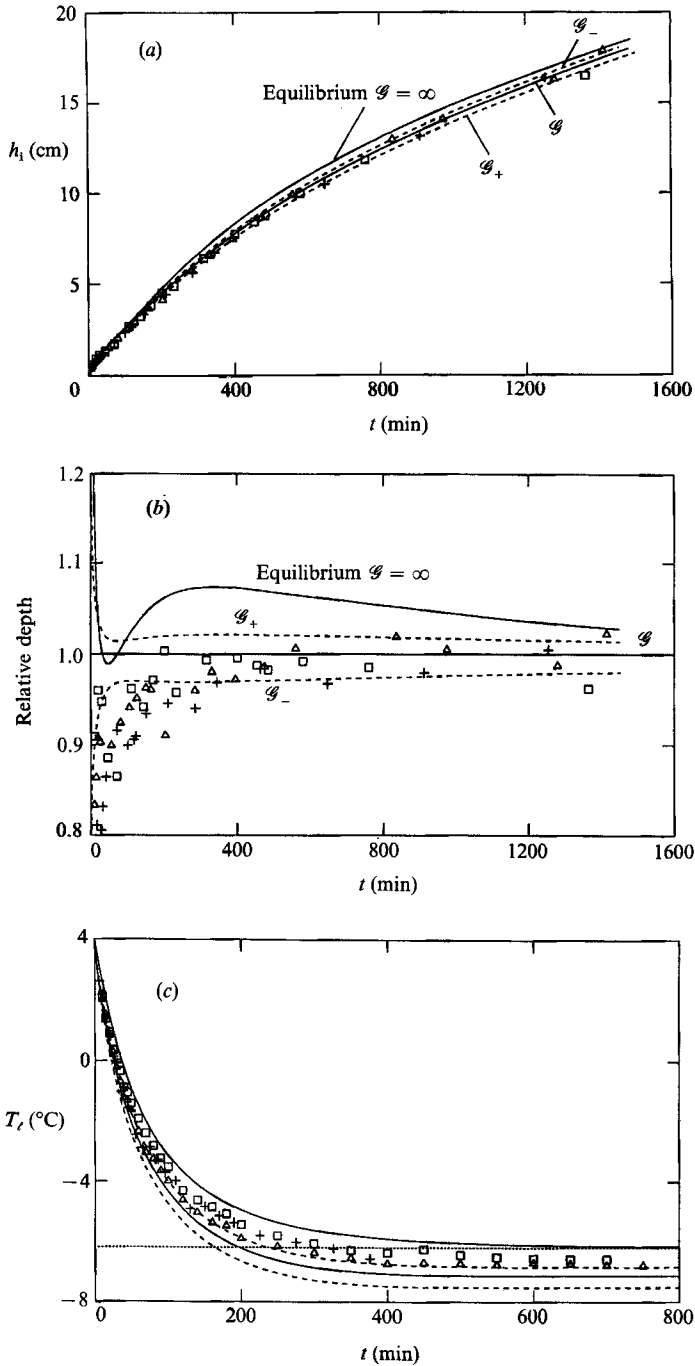


FIGURE 4. (a) The mush depth h_i , (b) the relative depth, and (c) the temperature of the solution T_l versus time. The symbols indicate the data obtained from the isopropanol experiments described in Part 1. The lower solid curve and the two dashed curves show the evolution predicted from the full theoretical model presented in §3, for the respective interfacial growth laws shown in figure 1. The upper solid curve in the figures shows for comparison the growth predicted by the simpler equilibrium model of Part 1. In (b) the depths shown in (a) have been rescaled by dividing by the depth predicted using our estimate of \mathcal{G} . The horizontal dashed line in (c) indicates the liquidus temperature of the solution (-6.2°C).

of the melt. Thus (3.12) shows that θ_ℓ is constant once convection ceases. The typical behaviour of the temperatures θ_i and θ_ℓ is illustrated in figure 3. The interface temperature is seen to rise rapidly from the imposed plate temperature $\theta = -1$ towards the liquidus temperature $\theta = 0$. It then evolves through both a local maximum and a local minimum. These two points mark the transitions in the thermal balances between conduction, the release of latent heat and convection that have been discussed in Turner *et al.* (1986) and in §4 of Part 1. At the same time, convection decreases the liquid temperature towards the interface temperature. Eventually, $\theta_\ell = \theta_i$, the convection ceases, and θ_ℓ remains fixed.

Our theoretical predictions for the isopropanol experiments of Part 1 are summarized in figure 4. We see that the theoretical prediction of the depth of the mushy layer is in very good agreement with the experimental data. For the temperature of the solution, the agreement is less satisfactory. However, most of the apparent discrepancy can be attributed to the effect of sidewall heating, which in Part 1 was observed to result in a steady-state temperature excess of about half a degree centigrade under our experimental conditions. We also note that our model can be simplified greatly, as is indicated in the Appendix, to yield an approximate global model of the mushy layer.

The major effect of introducing an interfacial growth law into our model is that it enables the model to predict correctly that the liquid will eventually become supersaturated. In the case of the isopropanol experiments, the occurrence of this supersaturation had a small influence on the growth of the mushy layer (as can be seen in figure 4*a*). The reason for this is that the magnitude of the supersaturation was always much less than the 5–7 °C that we found (in separate experiments) was necessary to nucleate new ice crystals. In some circumstances, however, the development of supersaturation can significantly affect the growth of the mushy layer by promoting the growth of additional crystals which release latent heat into the convecting melt. This effect can arise in a number of different situations. For example, it will occur if there are seed crystals present initially, if the crystals in the overlying mushy layer are heavy and fall, or if supersaturation develops that is sufficient to cause new crystals to nucleate. Such secondary crystallization is examined in detail in the next section.

4. Internal crystal growth

In the model presented in the previous section we noted the possibility that crystals can nucleate and grow in the convecting supersaturated fluid underlying the mushy layer. In this section, we describe an experiment in which such crystal growth occurred, and then proceed to extend our model to account for this situation.

The experiment used an aqueous solution of 33.0 wt % Na_2SO_4 (which corresponds to 74.8 wt % $\text{Na}_2\text{SO}_4 \cdot 10\text{H}_2\text{O}$), with an initial temperature of 40.0 °C. The solution was contained in a Perspex tank with horizontal dimensions 42 × 7.5 cm, which had a depth of 29 cm when the overlying brass plate was in place. The solution was cooled in the same manner as previously described for our isopropanol experiments (Part 1). We used a coolant precooled to –10 °C to achieve the desired plate temperature of –1.0 °C within 5 min. To minimize heat gains or losses from the laboratory, the tank was insulated using 5 cm thick styrofoam and the experiment was performed in a room whose temperature was adjusted to lie within about 2 °C of the temperature of the convecting solution. Crystals of $\text{Na}_2\text{SO}_4 \cdot 10\text{H}_2\text{O}$ nucleated after about 2 min, and by about 6 min a uniform mushy layer about 4 mm thick had formed. At these early

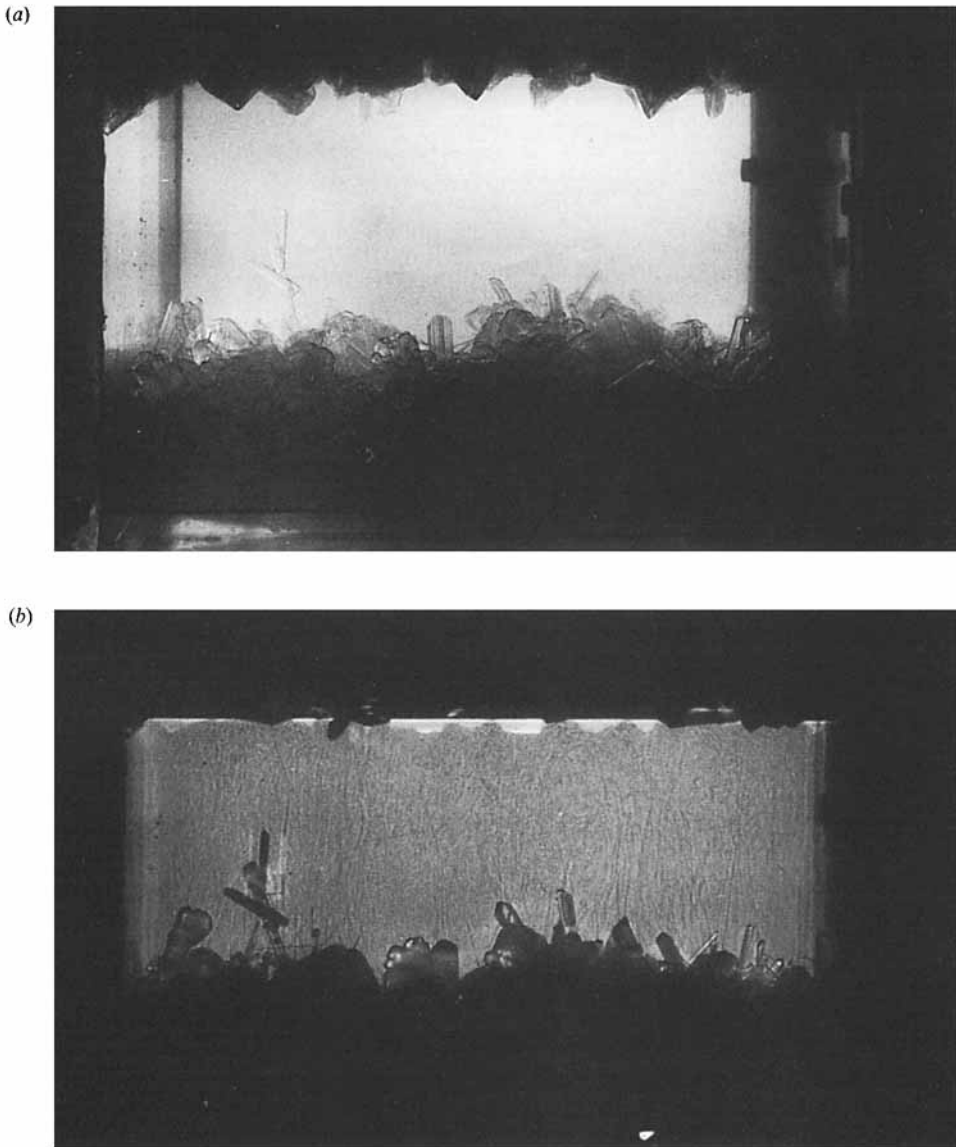


FIGURE 5. Photographs taken after 13 hours of an experiment in which an aqueous solution of Na_2SO_4 was cooled from above. The initial temperature, liquidus temperature and imposed plate temperature in this experiment were similar to the values used in the experiment described in §4. The experiment was performed in the apparatus displayed in figure 1 of Part 1. (a) A side view showing both the mushy layer and the layer of faceted $\text{Na}_2\text{SO}_4 \cdot 10\text{H}_2\text{O}$ crystals at the base of the tank. (b) A shadowgraph showing a sharp horizontal line which indicates the base of the strong compositional gradient through the mushy layer. Vigorous compositional convection from the growth of the basal crystals can also be seen.

times, the individual crystals were very small and densely spaced, and the mush appeared similar to the ice mush previously observed in our isopropanol experiments. After 100 min, the mushy layer had reached a depth of 2.3 cm and vigorous thermal convection had cooled the underlying solution down to its liquidus temperature of 32.0 °C. Small spiky crystals were observed growing on the base of the tank about 30 min later. It was not clear whether these crystals nucleated *in situ* or whether they had grown from very small crystals which may have fallen from the mush–liquid interface. The subsequent rapid growth of these basal crystals shown in figure 5(a) had two main effects. First, the resulting release of latent heat dramatically decreased the rate of fall of the solution temperature. Indeed, the rapid proliferation of basal crystals halted the fall in the solution temperature between 180 min and 280 min, and resulted in a slight rise in the solution temperature by 460 min. Secondly, the release of light, compositionally depleted fluid led to compositional convection (shown in figure 5b) which decreased the concentration of the melt and hence also its liquidus temperature.

An interesting feature of the experiment was that the fine, densely packed crystals observed in the mushy layer at early times grew to become large, faceted crystals later on (see figure 5a). This phenomenon, in which larger crystals grow at the expense of smaller ones, is known as ‘Ostwald Ripening’ (Glicksman & Voorhees 1984) and is an effect of surface energy. It becomes increasingly important as the rate of growth of the mush decreases (i.e. as the system approaches equilibrium), and arises in our experiments because the mushy layer generally grows more slowly as it becomes thicker. As a result, the crystals in the mushy layer become bounded by planes normal to the crystallographic directions in which the crystal growth is slowest (Kurz & Fisher 1986). The increasing thickness of the crystals, from less than 1 mm initially up to several cm near the end of the experiment, suggests that there is a significant surface energy associated with the contact between the crystals and the solution in the mushy layer. After about two days, only 9 large crystals protruded down to the mush–liquid interface. As a result, the position of this interface was most easily determined by using a shadowgraph to reveal the base of the compositional gradient through the mushy layer (see figure 5b). At the end of the experiment, we measured the temperature and composition of the solution at seven equally spaced heights in the mushy layer. We found that all these values plotted on the liquidus (to within experimental error). This apparent equilibrium over the large distances between the crystals could not have occurred by chemical diffusion alone, and must have been due to convection driven by small lateral variations of buoyancy in the interstices of the mushy layer.

Despite the increasing size of the crystals in the mush, we continue to treat it as a continuum, and focus our attention on how to extend the model developed in §2 to account for the growth of basal crystals. We begin by noting first that basal crystals grow in response to supersaturation in the convecting solution underlying the mushy layer and secondly that their growth decreases this supersaturation by releasing both latent heat and depleted fluid. We therefore propose to incorporate the growth of basal crystals in our model by assuming that they grow sufficiently rapidly to remove the supersaturation in the convecting solution. Hence the temperature of the liquid is given by its liquidus temperature

$$T_l = T_l(C_l). \quad (4.1)$$

Part of the phase diagram for the sodium sulphate–water system is shown in figure

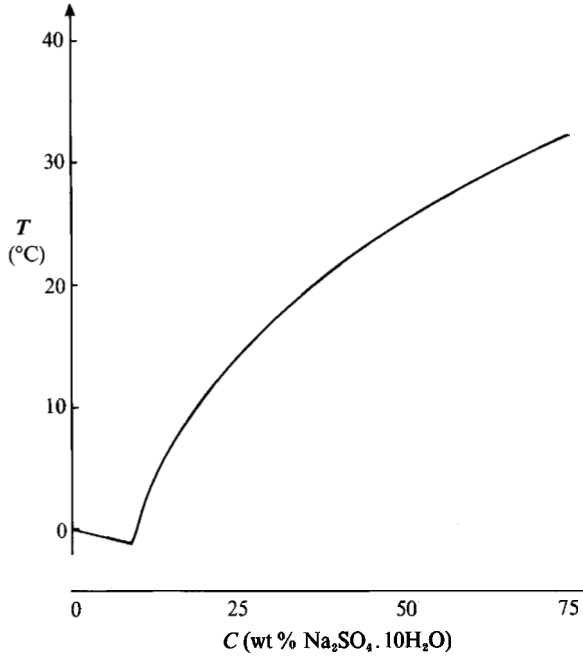


FIGURE 6. The phase diagram for the chemical system $H_2O-Na_2SO_4$, produced using data from Washburn (1926). The line plotted is the liquidus, which gives the temperature at which a given solution concentration is in thermodynamic equilibrium with either ice or crystals of $Na_2SO_4 \cdot 10H_2O$.

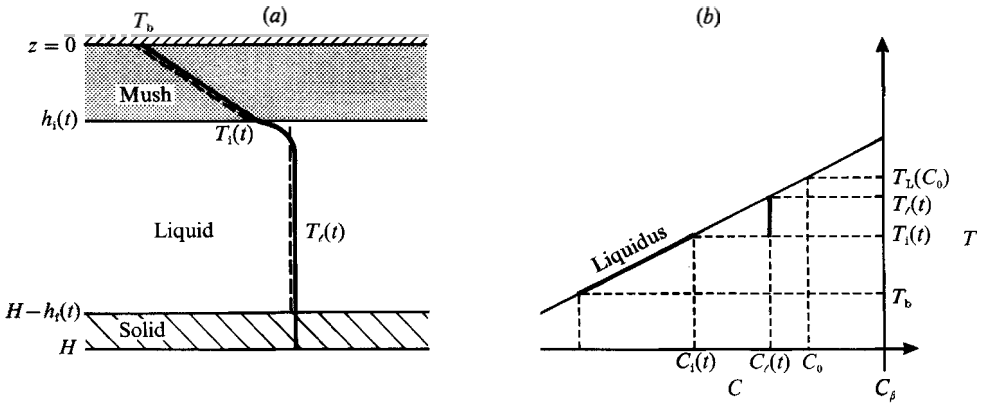


FIGURE 7. Definition sketches which, in the model developed in §4, replace those of figure 2 once the melt temperature reaches $T_L(C_0)$. Thereafter a solid layer of crystals grows on the base at a rate sufficient to keep the melt on the liquidus.

6. We no longer assume that the liquidus is linear but represent it numerically by a four-point cubic spline.

A schematic diagram of our theoretical model including the growth of crystals at the base of the container is shown in figure 7. A simplification in the model is that the crystals at the floor are envisaged to form a flat, solid layer of depth $h_f(t)$. By conservation of solute,

$$\frac{dh_f}{dt} = -\frac{(H-h_i-h_f)dC_f}{(C_p-C_f)} \tag{4.2}$$

If we assume that the basal solid has a uniform temperature equal to that of the solution, conservation of energy implies that

$$\mathcal{L} \frac{dh_r}{dt} - c_\ell(H - h_i - h_r) \frac{dT_\ell}{dt} - c_\beta h_r \frac{dT_\ell}{dt} = F_T, \quad (4.3)$$

where the four terms above are, respectively, the latent heat released by the growth of the basal crystals, the specific heats released by cooling both the solution and the basal crystals, and the heat flux into the mushy layer.

Equations (4.1)–(4.3) can be rewritten in the dimensionless forms

$$C_\ell = C_L(\theta_\ell), \quad (4.4)$$

$$\dot{h}_r = -\frac{(1 - h_i - h_r) dC_\ell}{(C_\beta - C_\ell) d\theta_\ell} \dot{\theta}_\ell, \quad (4.5)$$

and
$$\left\{ (1 - h_i - h_r) \left(1 + \frac{S}{C_\beta - C_\ell} \frac{dC_\ell}{d\theta_\ell} \right) + \frac{c_\beta}{c_\ell} h_r \right\} \dot{\theta}_\ell = -Nu(\theta_\ell - \theta_i)^{\frac{4}{3}}, \quad (4.6)$$

where C_L is the liquidus concentration defined by inverting (4.1). These equations replace the equations $C_\ell = C_0$, $\dot{h}_r = 0$ and (3.12) once the solution becomes supersaturated (i.e. once $T_\ell = T_L(C_0)$). In (4.6) the expression for the convective heat transfer F_T is unchanged from §3 since it is assumed to be unaffected by the compositional convection driven by the growing basal crystals.

Finally, to complete our extended model we recognize that, owing to the basal crystal growth, the composition of the solution incorporated into the mushy layer decreases with time. As a result the mean composition of the mushy layer C_H (including both liquid and solid phases) is now a function of height. This function is easily found since we have neglected vertical transport of solute within the mushy layer. Consequently, at each height z , it is given by the composition of the solution at time t_i when the position of the mush–liquid interface h_i was equal to z . This is expressed mathematically by

$$C_H(z) = C_\ell(t_i(h_i = z)) \quad (0 \leq z \leq h_i(t)). \quad (4.7)$$

We note that, in writing (4.7), we also assume that the convection in the underlying solution does not mix or entrain the stratified solution in the mushy layer. The solid fraction $\phi(z, t)$ at this height then depends on the local temperature $\theta(z, t)$ according to

$$\phi(z, t) = \frac{C_H(z) - C_L(\theta)}{C_\beta - C_L(\theta)}. \quad (4.8)$$

This expression for ϕ replaces (3.5) in the evaluation of (3.3), and (3.4) becomes

$$c = \phi \frac{c_\beta}{c_\ell} + (1 - \phi) + \frac{S}{C_\beta - C_H} \frac{dC_L}{d\theta} (1 - \phi)^2. \quad (4.9)$$

The typical behaviour of θ_i and θ_ℓ resulting from this system of equations is illustrated in figure 8. We see that the behaviour of both temperatures is identical to that shown in figure 3 until θ_ℓ reaches the liquidus. At this point, basal crystals begin to grow. The resulting release of latent heat produces discontinuities in the slopes of both temperature curves. Subsequently, the evolution of θ_ℓ indicates the slow decrease in the liquidus temperature due to the growth of basal crystals, while the evolution of θ_i towards θ_ℓ reflects the diminishing rate of growth of the mushy layer.

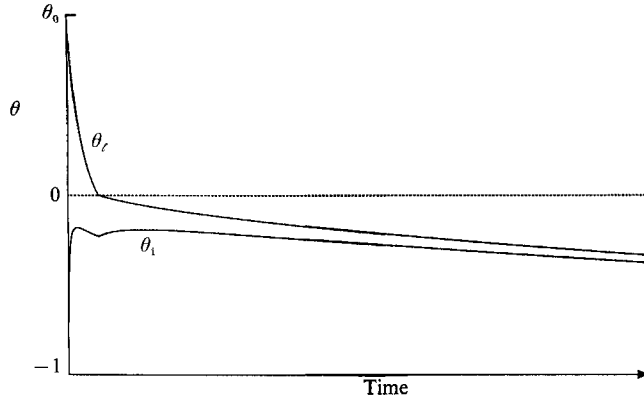


FIGURE 8. The schematic behaviour of the dimensionless temperatures at the interface and in the liquid, for the model presented in §4.

| Quantity | Value | Source |
|---------------|--|--------|
| c_β | $2.66 \text{ J cm}^{-3} \text{ }^\circ\text{C}^{-1}$ | B, D |
| c_l | $4.14 \text{ J cm}^{-3} \text{ }^\circ\text{C}^{-1}$ | C |
| k_l | $0.0059 \text{ W cm}^{-1} \text{ }^\circ\text{C}^{-1}$ | C |
| \mathcal{L} | 337 J cm^{-3} | C, D |
| ν | $0.03 \text{ cm}^2 \text{ s}^{-1}$ | C |
| α | $0.0006 \text{ }^\circ\text{C}^{-1}$ | C |
| λ | 0.056 | A |

TABLE 1. The parameter values used to calculate the evolution of the experiments with sodium sulphate. The data were obtained from the following sources: (A) Denton & Wood (1979), (B) Kaye & Laby (1973), (C) Washburn (1926) and (D) Weast (1971).

Further results were calculated using values for the physical constants appropriate for our experiment with Na_2SO_4 (table 1). Since the thermal conductivity of $\text{Na}_2\text{SO}_4 \cdot 10\text{H}_2\text{O}$ crystals could not be obtained from the literature, we determined its value by measuring the temperature difference across a known thickness of the crystals when a known heat flux was applied. The value obtained was $(0.8 \pm 0.1) \times 10^{-2} \text{ W cm}^{-1} \text{ }^\circ\text{C}^{-1}$.

The results are compared in figure 9 with our experimental data, which are indicated by the open circles. The solid and dotted curves shown on the graphs are calculated using linear interfacial growth laws for two different values of the kinetic growth parameter \mathcal{G} . For the dashed curves, we used the value of \mathcal{G} ($2.2 \times 10^{-4} \text{ cm }^\circ\text{C}^{-1} \text{ s}^{-1}$) that we have measured for isopropanol (represented by the solid line in figure 1), while for the solid curves we used the smaller value $1.5 \times 10^{-4} \text{ cm }^\circ\text{C}^{-1} \text{ s}^{-1}$. From figure 9(a), we find that the former value of \mathcal{G} overpredicts the rate of growth of the mushy layer and underpredicts the growth of the basal solid. In comparison, the solid curves indicate that a value of \mathcal{G} can be chosen to give good agreement with the experimental results. The fact that the appropriate value of \mathcal{G} is smaller for Na_2SO_4 than it is for ice is not surprising since larger undercoolings are typically required for the growth of faceted crystals with significant surface energies (Kurz & Fisher 1986). We also note that although only about 15% of the melt remains by 4000 min, the Rayleigh number at this time is still large (3.8×10^5) and hence the convection is still fairly vigorous.

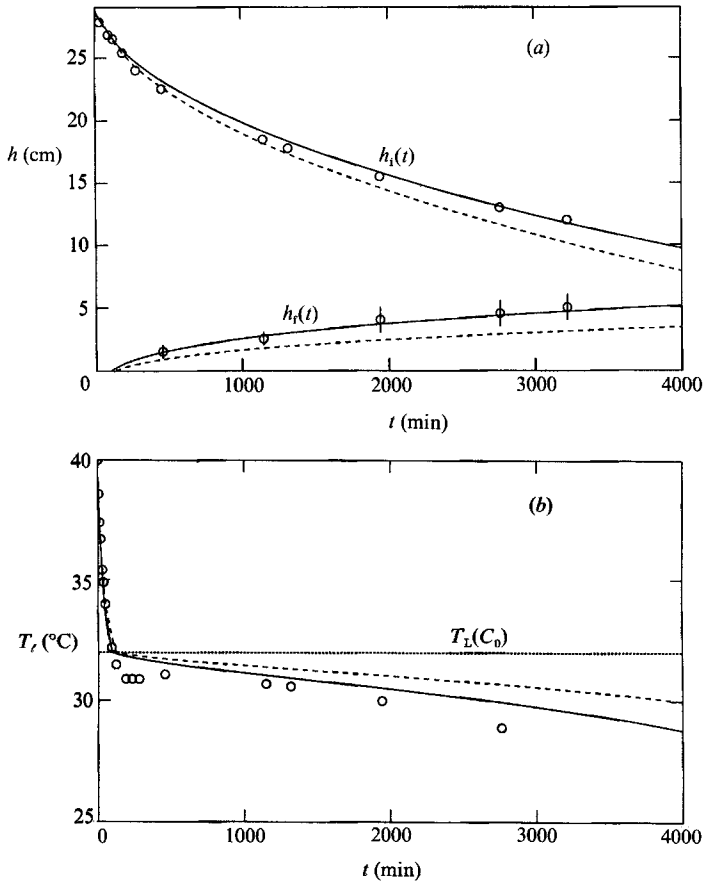


FIGURE 9. (a) The depths of mush (h_i) and basal solid (h_b), and (b) the temperature of the solution T_l versus time. The open circles indicate the results of our experiment with Na_2SO_4 , and the curves show the evolution predicted from the theoretical model developed in §3. The dashed curves were calculated using a linear interfacial growth law with the proportionality constant \mathcal{G} appropriate for isopropanol (corresponding to the solid line in figure 1). The solid curves indicate that a smaller value for \mathcal{G} can be chosen to fit the experiments more accurately. The size of the error bars in (a) shows the considerable uncertainty in estimating the mean depth of basal solid. The broken horizontal line in (b) indicates the liquidus temperature of the solution (32.0 °C).

Figure 9(b) shows that the evolution of the temperature in the solution is also in reasonable agreement with our model. In particular, the time taken for the solution to reach saturation is accurately predicted. The subsequent agreement is poorer, though it improves as the supersaturation in the solution (assumed to be zero in our model) decreases, owing both to the declining heat flux F_T into the mushy layer, and to the rapid increase in the surface area of crystals growing on the base of the tank.

5. Discussion and conclusions

A simple kinetic growth law relating the rate of advance of a mush–liquid interface to the local supercooling was introduced in §2 and employed in subsequent sections to develop models of a binary alloy being cooled from above. Very good agreement between the results of the models and data from laboratory experiments has been

achieved. This suggests that we have correctly identified and quantified the physical processes involved in such solidifying systems.

Our models have certain features, such as the structure of the mushy layer and the use of a kinetic growth law, in common with a model developed by Flood & Hunt (1987) for the casting of metallic alloys. The main differences lie in our expressions for the convective heat flux F_T from the liquid region to the mushy layer and in our treatment of the secondary solidification. Flood & Hunt (1987) do not consider the nature of the convective flow in the liquid. The associated heat flux F_T is simply taken to be proportional to the temperature difference between the interior of the melt and the mush-liquid interface, with a constant heat-transfer coefficient chosen to give freezing times comparable with those observed in their experiments. This representation of F_T is sufficient to investigate some qualitative features of the solidifying system. However, for quantitative predictions, the nature of the convection and the resulting heat flux must be known explicitly.

In this series of papers, we have confined our attention to high-Rayleigh-number convection in one particular geometry, that of cooling from above. We have been able to employ a specific expression for F_T in terms of known fluid properties and have achieved good agreement with experimental observations. Our models predict that the melt becomes supersaturated, which causes further solidification away from the cooled boundary. Flood & Hunt (1987) consider that this secondary solidification takes the form of equiaxed crystals (mushy spheres) suspended in the melt. These spheres accommodate the residual fluid, that they produce as they grow, within their own interstices, and so there is no global redistribution of solute in the system. At the opposite extreme, we have considered a case in which the secondary crystals are compacted in a solid layer at the base of the container and release all their residual fluid into the overlying, convecting liquid. Either extreme, or something between the two, may occur in different situations. Our picture seems appropriate for the particular experiments with sodium sulphate that we performed. In order to obtain a better understanding of what is appropriate in general, detailed studies of the compositional convection that can transport residual fluid away from the growing crystals, perhaps along the lines of Woods & Huppert (1989), are needed.

There are important geological implications of the present study, for example in the understanding of how lava flows cool and solidify. Basaltic lava lakes, cooled by the air (Turcotte & Schubert 1982), and komatiitic lavas ponded on the sea floor (Turner *et al.* 1986), are two examples in which the strongest cooling is from above and where the viscosity of the magma is sufficiently low for them to convect vigorously. Equilibrium models of solidification, such as that in Part 1, will accurately predict the removal of any superheat from the lava and the initial formation of a dendritic crust. However, in these models, the crust buffers the interior of the lava from convectively cooling below its initial liquidus temperature. In contrast, the present models show that disequilibrium effects can cause additional crystallization of the lava, either at the base of the flow or in its interior. This secondary solidification can effect a change in the composition of the lava, which lowers the liquidus temperature and allows cooling and convection to continue.

In fact, vigorous convection can occur in a magma chamber even where there is no initial superheat. In such a case, there can be a competition between the growth of the thermal boundary layer by diffusion before convective instability, and the decrease of the kinetic undercooling which provides the driving buoyancy for convection. A dimensional analysis of this competition was outlined by Kerr *et al.*

(1989), who showed that vigorous convection would take place during a substantial fraction of the evolution of the chamber provided that

$$\frac{\alpha g H^2}{\mathcal{G}_v} \gg Ra_c, \quad (5.1)$$

where $Ra_c (\approx 10^3)$ is the critical Rayleigh number for the onset of convection.

Another consequence of this study is that it shows how disequilibrium, coupled with convective mixing, can cause the composition of the melt to evolve with time. This results in a stratification of the mean composition of the mushy layer as given by equation (4.7). This behaviour also provides a mechanism for the redistribution of solute during the complete solidification of an alloy cooled from above. Such compositional stratification, which is observed in completely solidified ingots and in igneous rocks, is analysed in Part 3 of this series.

We wish to thank Mark Hallworth for his technical assistance with the laboratory experiments. A. B. Crowley, J. Dantzig, A. Hoadley, D. Hurle, C. Jaupert and J. S. Turner provided valuable comments and reviews. We gratefully acknowledge research fellowships from the following Cambridge Colleges: Churchill (R.C.K.), Trinity (M.G.W.) and St John's (A.W.W.), and financial support from the BP Venture Research Fund (H.E.H.). A.W.W. is also grateful for support as a Green Scholar at IGPP, Scripps Institution of Oceanography during the final stages of the research.

Appendix

Further to the Appendix of Part 1, we examine the effect of using an interfacial growth law in a bulk model of the mushy layer. We begin by adopting the trial function

$$\phi = \phi(t) \quad (0 \leq z \leq h_1), \quad (A 1)$$

so that the solid fraction is independent of spatial position. Instead of the linear temperature profile assumed in Part 1, we approximate the temperature field by a function that is consistent with (A 1) in the limit of large Stefan number. In this limit, there is a balance between conduction and production of latent heat, and the equation for heat convection in the mushy layer (3.2) can be integrated to give, in dimensionless terms,

$$\theta = -1 + (1 + \theta_1) \frac{z}{h_1} - \frac{S}{2k} \dot{\phi} z(z - h_1). \quad (A 2)$$

We see that the linear profile is modified by a quadratic term due to the internal release of latent heat. Global conservation of solute yields the dimensionless constraint

$$(1 - \phi) \frac{1}{h_1} \int_0^{h_1} \theta \, dz + \phi \mathcal{C} = 0, \quad (A 3)$$

which when evaluated using (A 2) gives

$$\dot{\phi} = \frac{6k}{Sh_1^2} \left\{ -\theta_1 + \frac{\phi_e - \phi}{\phi_e(1 - \phi)} \right\}, \quad (A 4)$$

where

$$\phi_e = \frac{1}{2\mathcal{C} + 1} \quad (A 5)$$

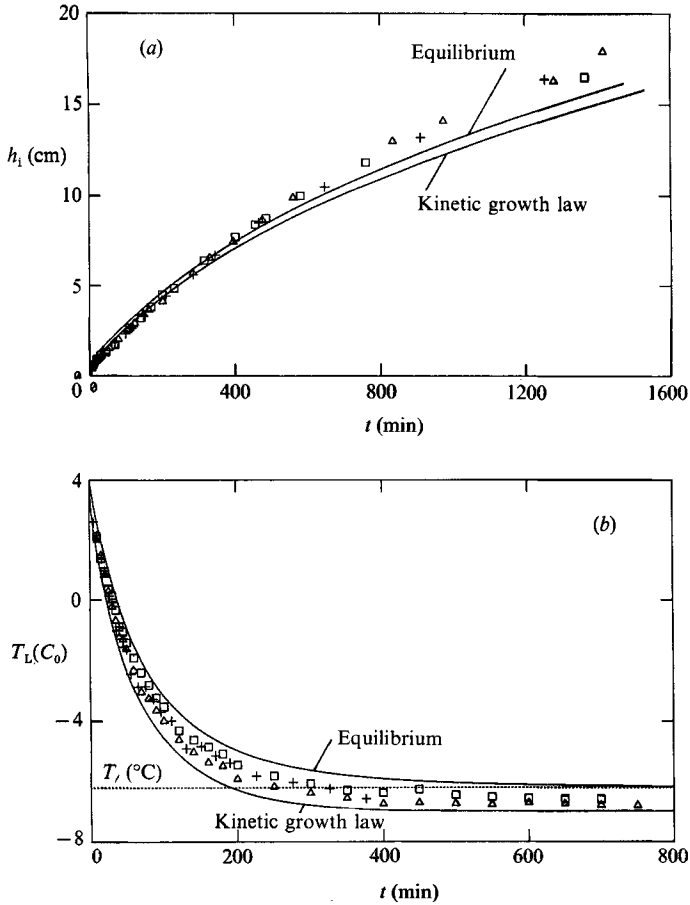


FIGURE 10. (a) The mush depth h_i and (b) the temperature of the solution T_i versus time. The symbols indicate the data obtained from our isopropanol experiments. In comparison, the curves denote the evolution predicted by the simple bulk model outlined in the Appendix, assuming either that the interfacial temperature lies on the liquidus (upper curve) or is given by the intermediate growth law shown in figure 1 (lower curve). The horizontal dashed line in (b) indicates the liquidus temperature of the solution (-6.2 $^{\circ}\text{C}$).

is the solid fraction for a mush in equilibrium with the liquid region such that $\theta_i = 0$ and $\dot{\phi} = 0$. A full set of *ordinary* differential equations describing the system are (A 4), (3.10), (3.12) and

$$\{S\phi + (\theta_r - \theta_i)\} \dot{h}_i = k \frac{(1 + \theta_i)}{h_i} - \frac{1}{2} S h_i \dot{\phi} - Nu(\theta_r - \theta_i)^{\frac{4}{3}}, \quad (\text{A } 6)$$

which is the equivalent of (3.11), having used the trial function (A 2) to estimate the temperature gradient at the edge of the mushy layer. These are subject to the initial conditions $h_i = 0$, $\theta_r = \theta_0$, $\theta_i = -1$ at $t = 0$. Note that these initial conditions imply that $\phi = 1/(1 + \mathcal{C})$ at $t = 0$, which allows $\dot{\phi}$ to be finite according to (A 4).

The differential equations were solved using a fourth-order, Runge-Kutta method starting from asymptotic expansions of the solutions. The results are shown in figure 10 in comparison with both our experimental data and our calculations based on an equilibrium interfacial condition from Part 1. We find that both bulk models yield

reasonable results. We also observe that, as was the case in our local models of the mushy layer, the incorporation of the interfacial growth law slightly retards the growth of the mushy layer.

REFERENCES

- CARSLAW, H. S. & JAEGER, J. C. 1959 *Conduction of Heat in Solids*. Oxford University Press.
- CHEN, C. F. & TURNER, J. S. 1980 Crystallization in a double-diffusive system. *J. Geophys. Res.* **85**, 2573–2593.
- DENTON, R. A. & WOOD, I. R. 1979 Turbulent convection between two horizontal plates. *Intl J. Heat Mass Transfer* **22**, 1339–1346.
- FLOOD, S. C. & HUNT, J. D. 1987 A model of a casting. *Appl. Sci. Res.* **44**, 27–42.
- GLICKSMAN, M. E. & VOORHEES, P. W. 1984 Ostwald ripening and relaxation in dendritic structures. *Metall. Trans.* **15**, 995–1001.
- HUPPERT, H. E. & WORSTER, M. G. 1985 Dynamic solidification of a binary melt. *Nature* **314**, 703–707.
- KAYE, G. W. C. & LABY, T. H. 1973 *Tables of Physical and Chemical Constants and some Mathematical Functions*. Longman.
- KERR, R. C., WOODS, A. W., WORSTER, M. G. & HUPPERT, H. E. 1989 Disequilibrium and macrosegregation during the solidification of a binary melt. *Nature* **340**, 357–362.
- KERR, R. C., WOODS, A. W., WORSTER, M. G. & HUPPERT, H. E. 1990*a* Solidification of an alloy from above. Part 1. Equilibrium growth. *J. Fluid Mech.* **216**, 323–342.
- KERR, R. C., WOODS, A. W., WORSTER, M. G. & HUPPERT, H. E. 1990*b* Solidification of an alloy from above. Part 3. Compositional stratification within the solid. *J. Fluid Mech.* **218**, 337–354.
- KURZ, W. & FISHER, D. J. 1986 *Fundamentals of Solidification*. Trans. Tech. Publications.
- TURCOTTE, D. L. & SCHUBERT, G. 1982 *Geodynamics*. John Wiley & Sons.
- TURNER, J. S., HUPPERT, H. E. & SPARKS, R. S. J. 1986 Komatiites II: Experimental and theoretical investigations of post-emplacement cooling and crystallization. *J. Petrol.* **27**, 397–437.
- WASHBURN, E. W. (ED.) 1926 *International Critical Tables of Numerical Data: Physics, Chemistry and Technology*. National Academic Press.
- WEAST, R. C. (ED.) 1971 *CRC Handbook of Chemistry and Physics*. The Chemical Rubber Co.
- WOODS, A. W. & HUPPERT, H. E. 1989 The growth of compositionally stratified solid above a horizontal boundary. *J. Fluid Mech.* **199**, 29–53.
- WORSTER, M. G. 1986 Solidification of an alloy from a cooled boundary. *J. Fluid Mech.* **167**, 481–501.